3-D Range Imaging Using Stripe-Like Illumination and SPAD-Based Pulsed TOF Techniques

Lauri Hallman ⬤, Sahba Jahromi ⬤, Jussi-Pekka Jansson ⬤, Pekka Keränen ⬤, and Juha Kostamovaara ⬤, *Life Senior Member, IEEE*

Abstract—A solid-state three-dimensional (3-D) range imager using the pulsed time-of-flight principle and a single photon avalanche diode (SPAD) based receiver is demonstrated. Contrary to conventional flood illumination, the suggested system uses sequentially scanned illumination stripes to increase the irradiance under the measured field of view and to reduce the receiver complexity. At equal average illumination power levels this approach increases the signal-to-noise ratio in the receiver enabling thus longer range and/or better performance in high background illumination conditions, albeit at the cost of lower transversal resolution. The transmitter uses eight sequentially driven laser diodes, each of which produces an optical pulse power, length and wavelength of $\sim$50 W, 2 ns and 905 nm, respectively at a pulse rate of $\sim$30 kHz so that the total effective pulsing rate is $\sim$250 kHz and the average illumination power is $\sim$30 mW. 3-D imaging is demonstrated outdoors in over 50 klux ambient lighting up to $\sim$10 m distance with 15 Hz frame rate and mm–cm level longitudinal precision in a field of view of about 40×10 degrees. The transversal resolution of the system is 16×128 pixels. The measurement results show 3-D measurement precision scaling according to the laser pulse width and averaging.

Index Terms—Laser radar, LiDAR, range imaging, single photon detection.

I. INTRODUCTION

THREE-DIMENSIONAL (3-D) range imaging techniques have a lot of applications in autonomous vehicles, robotics, small vehicle guidance, (unmanned aerial vehicles, UAVs), virtual/augmented reality (VR/AR) and machine control (e.g., construction and forestry machines) [1], [2]. Several groups have been working to develop 3-D range imaging devices in solid-state, i.e., with no moving parts, to increase durability and to reduce costs and device size. One approach to solid-state 3-D range imaging uses a modulated continuous wave (CW) laser beam and calculates the distance information from the phase difference between the emitted and received signal with a CMOS active pixel sensor [3]. This technology achieves high image pixel resolution, but at the cost of a limited measurement range and a relatively high average optical illumination power (hundreds of milliwatts) [4].

Another promising solid-state technique for 3-D range imaging uses a 2-D CMOS single photon avalanche diode (SPAD) detector array to directly measure the round-trip transit times of the photons of a short laser pulse sent from the transmitter to the target. Most demonstrations of such devices using the pulsed time-of-flight technique (TOF) are based on flood illumination strategy, i.e., the laser power is spread to illuminate the full field of view (FOV) of the system for every laser pulse emitted [5], [6], [7], [8], [9], [10], [11], [12], [13], [14]. 3-D range imagers using flood illumination tend to have low maximum measurement distance outdoors since background induced noise photon counts typically impede signal counts in SPAD (single photon avalanche diode) based imaging. Block-based imaging has been suggested to alleviate this problem, as focusing of all the laser power on a part of the image at a time increases the SNR (signal-to-noise ratio) of the particular pixels so that the performance is increased despite measuring only a part of the FOV at a time [15], [16], [17]. Also, the receiver circuit is simplified since the SPADs can share TDCs (time-to-digital converters).

In this work, we develop the block-based illumination concept further by using an array of edge-emitting laser diodes and optics to create a stripe-like illumination pattern with the transmitter. One of the stripes (and thus one of the laser diodes) is activated at a time so that the FOV of the imager is sequentially electrically scanned over with the illumination stripes. The use of illumination stripes, instead of homogenous illumination (even in blocks), enables one to increase the irradiance at the target albeit at the cost of spatial resolution (at longer ranges) [18]. As explained in more details in Section II, this improves the range performance especially at longer ranges in high background illumination conditions, which is important in many practical measurement applications, e.g., with construction and forestry machines [19], [20].

This study presents the realization and characterization of a solid-state 3-D imager that measures distances using pulsed time-of-flight. This device uses stripe-based illumination in the transmitter and a 2-D CMOS SPAD/TDC receiver. The focus of the paper is on the details of the transmitter, including the electronic components and the creation of the light pattern. It also discusses the achievable range imaging performance under different lighting conditions. The details of the receiver

Lauri Hallman, Jussi-Pekka Jansson, and Juha Kostamovaara are with Circuits and Systems Research Unit, University of Oulu, 90014 Oulu, Finland (e-mail: lauri.hallman@oulu.fi; jussi.jansson@oulu.fi; juha.kostamovaara@oulu.fi).

Sahba Jahromi is with Murata Electronics Oy, 01620 Vantaa, Finland (e-mail: sahba.sabetghadam-jahromi@murata.com).

Pekka Keränen is with Noptel Ltd., Teknologiantie 2, 90570 Oulu, Finland (e-mail: pekka.keranen@noptel.fi).

Digital Object Identifier 10.1109/JPHOT.2024.3373069

electronics can be found in another study [16]. The blocks of the measurement system are detailed in Section II. Section III shows the measurement results demonstrating the performance of the resulting 3-D range imaging. The results are discussed and compared with those of other relevant studies in Section IV.

II. MEASUREMENT SYSTEM

A. Topology of the Measurement System

The 3-D range imagers based on pulsed TOF technique and SPAD receiver techniques typically utilize flood illumination techniques, where the full field of view of the system is illuminated with every laser pulse. This kind of an illuminator is simple to realize e.g., with a VCSEL laser diode array and a diffuser. Flood illumination works well at short distances (up to a few meters) and in low background illumination conditions [21]. However, at longer measurement ranges and higher background illumination conditions ($>$10 klux), as suggested in earlier research e.g., in [15], [16], [17], [22] it may be beneficial to illuminate the system FOV sequentially so that only a portion of the FOV is illuminated at a time, i.e., per single emitted laser pulse. The reason for the performance improvement is that in this way the irradiance on the target segment under illumination is higher by a factor of the number of segments used while having the same total average illumination power. Thus, also the signal photon detection probability is higher in the receiver by the same proportion (assuming that the signal photon detection probability for a single pulse is $<$1 which typically is the situation). This will result in improved performance, since a lower number of laser pulses is needed for the required number of valid signal counts. Thus, the number of random noise counts due to background radiation is also lower and the SNR (signal-to-noise ratio) is correspondingly improved.

In this work, the above reasoning has been applied and extended in such a way that instead of homogenously illuminated segments, the system field of view is illuminated sequentially by stripes, i.e., the vertical dimensions of the illumination segments have been shrunk to a practical minimum. This increases the irradiance on the respective SPAD detectors in the receiver and thus further improves the SNR.

The price paid is lower transversal resolution (limited by the number of separate laser illumination stripes) since the regions between the stripes are practically not illuminated and thus are usually skipped in the measurement cycle. In some measurement scenarios, however, especially at lower measurement ranges, the inevitable stray laser light illuminates the regions between the stripes sufficiently enabling measurement also there, as is shown later in Section III.

A laser diode transmitter utilizing segmented illumination (either in blocks or stripes) is more complicated than a flood illuminator especially since in any case energetic and high-speed laser pulses need to be generated for range measurement of more than a few meters in bright sun light. This added complication is partly compensated for in the receiver, which, due to the sequential illumination, needs time-to-digital converter (TDC) units only for the SPADs under illumination. Thus, a smaller number of TDCs are needed since they can be shared between the sequentially illuminated blocks.
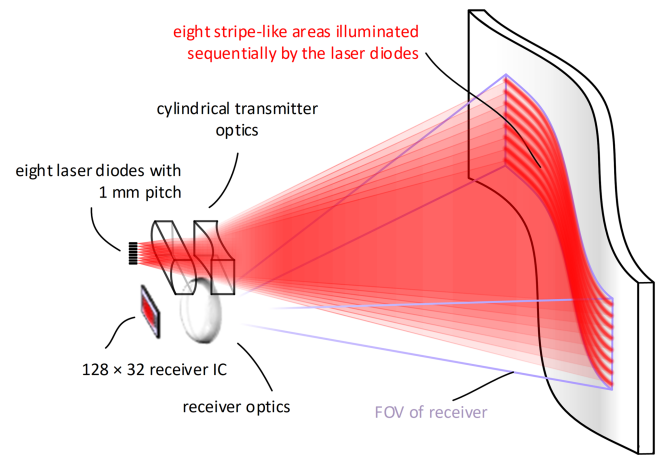

Fig. 1. Measurement setup.

In the demonstration realization of this work, eight pulsed laser diodes and simple cylindrical optics (Fig. 1) were used to illuminate eight stripe-like areas (blocks) in the system FOV. The laser beams were collimated in the vertical directions by the first element in the optics of Fig. 1 and spread in the horizontal direction to illuminate the FOV of every second SPAD row pair. The angular separation between the illuminated stripes was about 25 mrad since the pitch of the laser diodes was 1 mm and the collimating cylindrical lens had a focal length of 4 cm. The receiver used optics with a focal length of 6.7 mm, an f number of 1.2 and an optical 43 nm bandpass filter centered at 900 nm. The receiver IC had a 128×32 matrix of SPAD detectors with 40 μm pitch and 257 time-to-digital converters (TDC) to measure time intervals between start-signals from the laser pulse emissions and the first stop-signals arising from photon detection or noise from each SPAD detector. 256 TDCs (in addition, one TDC was needed for the start signal, i.e., laser pulse emission) could be electrically connected to any two adjacent SPAD rows for a selected time [16]. Gating of the SPADs was also possible, meaning that the SPADs could be switched on (biased above the threshold voltage) at a selected time after the laser emission to reduce the probability of SPAD receivers from getting blocked by noise detections (i.e., random background hits produced by sun light, for example) before the signal.

B. Laser Transmitter Matrix

Two different types of edge emitting double heterostructure laser diodes from two manufacturers were tested, four of both types were used in the transmitter. The assembly of the laser diode chips on the transmitter printed circuit board is shown in Fig. 2(c). The specifications of the laser diodes were similar: both laser diode types had three nano-stacked emitters with about 70 W/A total responsivity and $\sim$905 nm peak emission wavelength. The main difference was the narrow 110 μm emitter width of type A compared to the 220 μm emitter width of type B. The laser pulse emission times had about 500 ps static offset, see Fig. 2(d), probably due to GaNFET driver propagation delay variations, which were compensated for in the measurement results. The width of the laser pulses (full width at half maximum, FWHM) was about 2 ns and the pulse energy $\sim$110 nJ, see Fig. 2(d). Each

(a)

(b)

type A   type B

(c)

output power (W)

FWHM = 2.0 ns ... 2.13 ns
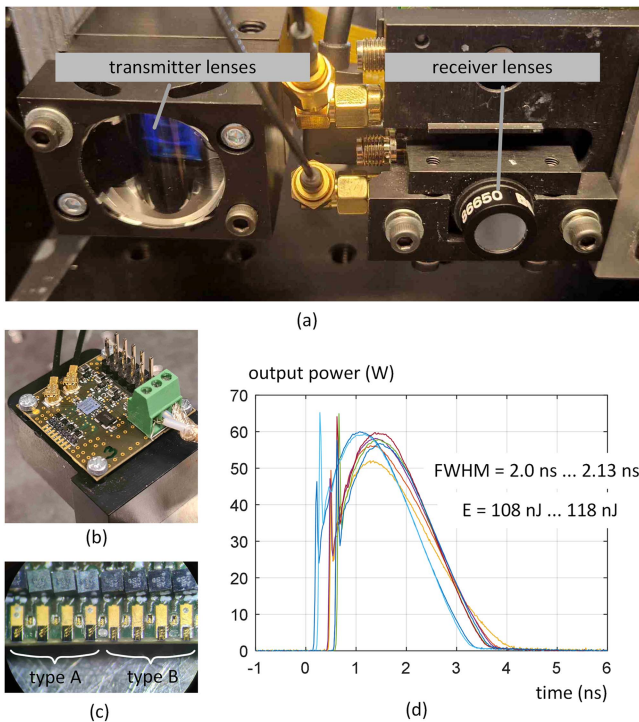
E = 108 nJ ... 118 nJ

time (ns)

(d)

Fig. 2. (a) Photograph of the optics of the measurement device. (b) The laser transmitter circuit board. (c) A close-up zoom of the laser diodes in the laser transmitter. (d) Laser output waveforms of the eight laser diodes.

of the laser diodes were driven with a GaN driver at a pulsing rate of ~31 kHz (one at a time). The 8 laser diodes were driven one after another so that the total pulse rate was 250 kHz. The GaN drivers use similar circuit techniques as in [15], however the pulse energy was scaled up by using nanostack laser diodes. Thus, the average optical illumination power of the transmitter was ~30 mW.

III. MEASUREMENT RESULTS

3-D measurements were performed in several scenarios to characterize the measurement performance. In many applications over 10 Hz frame rate is preferred, and therefore in the first measurement 2048 laser shots were fired per laser at a pulsing frequency of 250 kHz, leading to an equivalent frame rate of 15 Hz (= 250 kHz/8/2048). In the current setup, TOF histograms from SPADs were processed afterwards in Matlab to produce the 3-D images.

Three measurement cases were used to demonstrate the available performance of the setup in the measurement environment presented in Fig. 3. The background illumination in the sunlit area of the scene was approximately 50 klux. This was measured from the target surface using a Hioki FT3425 lux meter, which was aimed towards the 3-D imager.

A. Signal-to-Noise in Detection

In the first measurement case SPAD gating starting at 4 m was used. The 3-D measurement result in Fig. 4(a) shows that in this case the SNR is sufficient ($\gtrsim 3.7$) only in the shaded parts of the wall. SNR is defined here as the ratio of the filtered signal

Fig. 3. Photograph of the first test scene: A white partially shaded wall outdoors with the laser illumination pattern illustrated. Two specific measurement spots are marked with circles, which are examined in Fig. 5.

amplitude divided by the square root of the signal variance. The filtering and SNR calculation are explained in [15], [17].

In the second case, an optical 0.4 ND (neutral density) attenuator was added at the receiver. Perhaps counterintuitively the 3-D result in Fig. 4(b) is better in this case. This is due to a decrease in the blocking effect especially in sunny parts of the scene, which is shown and explained in more detail in Fig. 5. Only a few pixels show distance results from the leaves (at a distance of ~6 m) in the low part of the image due to a large background count rate from the leaves (the mean time interval τ_{BG} between random detections in the SPADs is about 30% smaller from the leaves compared to the white wall due to the specular reflections from the leaves).

In the third case, the start of the gating was shifted later to 7 m leading to a yet better result shown in Fig. 4(c). Most pixels now show a result even from the sunny area. The lowest SPAD row, on the other hand, shows only a few 3-D results mainly due to blocking by the leaves at the bottom of the image.

In all of the above cases, not many 3-D results were obtained from the FOV edges due to a shift of the optical bandpass to lower wavelengths, below the laser wavelength of 905 nm, for large angles of incidence. The bandpass filter would be less sensitive to the view angle if it would be placed between the optics and the SPAD receiver, but prototyping constraints forced the bandpass filter to be placed in front of the optics. Alternatively, bandpass filters designed especially for large degrees of incidence can be used.

Fig. 5 explains the enhanced quality of 3-D images achieved through optical attenuation and gating. It displays SPAD time-of-flight count histograms for the sunny and shady spots marked in Fig. 3, in Fig. 5(a) and (b), respectively. The improvement is linked to the receiver circuit's design, where the TDCs are limited to a single trigger per laser pulse. This restriction leads to an exponential decay in the background count histogram (assuming Poisson statistics) roughly following [23], [24], [25]

$$e^{-\Delta t_{\mathrm{flight}}/\tau_{\mathrm{BG}}}, \qquad (1)$$

where $\Delta t_{\mathrm{flight}}$ is the photon flight time after start of gating.

A very high background detection rate (a low τ_{BG}) can also diminish the chance of signal detection and therefore, for
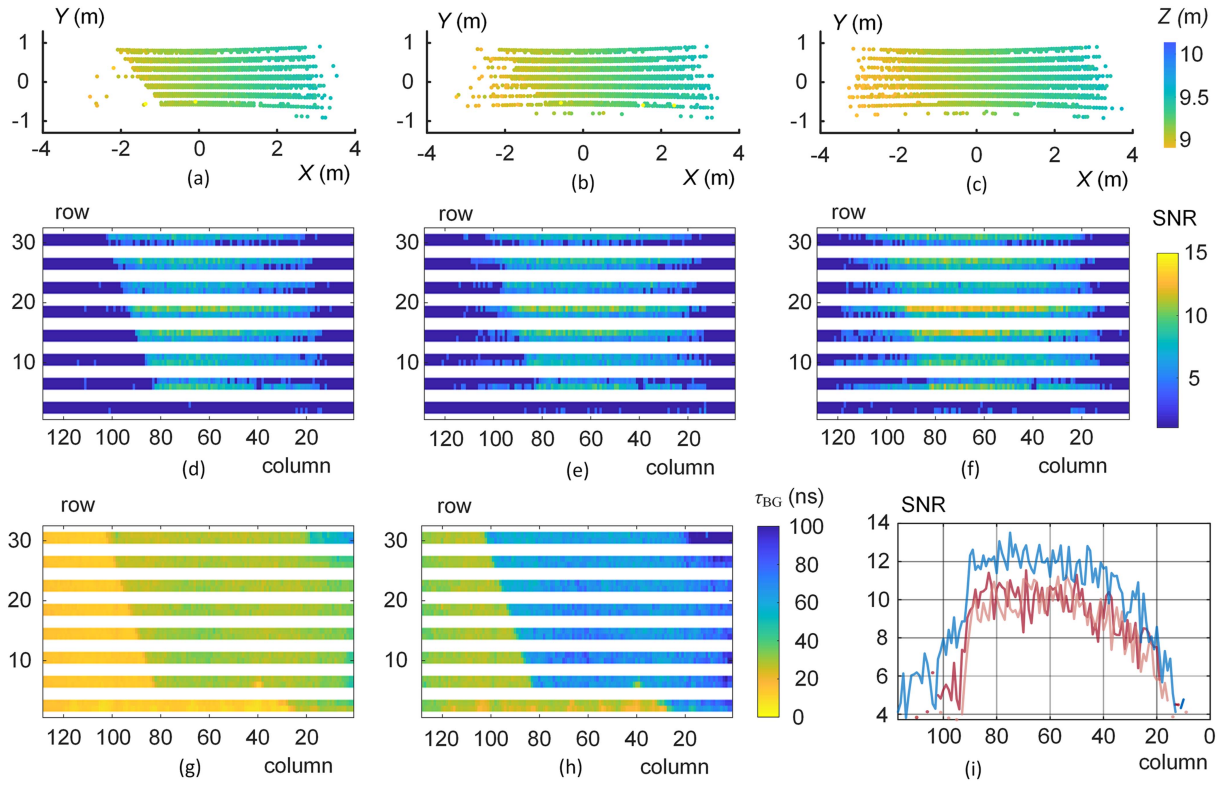
Fig. 4. 3-D point cloud measurement results of the scene shown in Fig. 3 measured with SPAD gating starting (a) case 1: At 4 meters (b) case 2: At 4 meters with an 0.4 neutral density (ND) filter at the input of the receiver and (c) case 3: Gating starting at 7 meters and an 0.4 ND filter at the input of the receiver. (d)–(f) SNR for each pixel for cases 1, 2 and 3, correspondingly. τ_{BG} for each pixel (g) without and (h) with the 0.4 ND filter. (i) SNR for row number 24, light red: Case 1, dark red: Case 2, blue line: Case 3. 2048 laser shots per row pair were used in all measurements leading to an equivalent frame rate of 15 Hz. The background illumination in the sunny part of the scene was 50 klux in all cases.
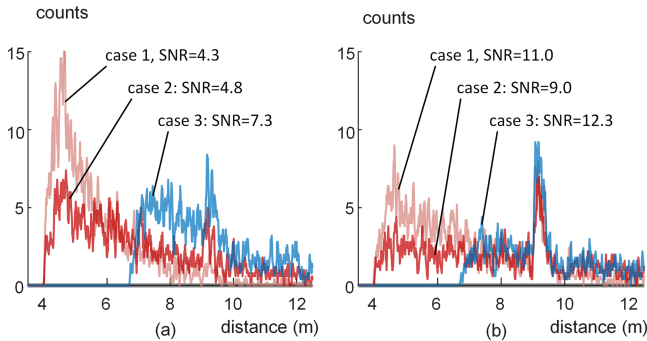

Fig. 5. Smoothed SPAD count histograms measured from (a) the left circled spot on the sunny part of the wall and from (b) the right circled spot on the shady part of the wall shown in Fig. 3.

example, in Fig. 5(a) the signal peak at ~9 m is visibly larger when an input ND attenuator is used in case 2 compared to case 1 without an input ND attenuator. Specifically, in case 1 in Fig. 5(a) the histogram decays to $1/e \approx 37\%$ in about 2 meters which corresponds with a to and fro flight time of about 13 ns (same value as in Fig. 4(g) in the sunny part in the image). The significance of the decay is that, for example, after a time period τ_{BG} following the gate's start, the effective photon detection probability drops to only 37% of its initial value at the beginning of gating and continues to decrease exponentially. In case 1 the

effective photon detection probability has decreased by a factor of 25 due to the exponential decay at the signal arrival time. On the other hand, in case 2 the use of the ND filter approximately halves the optical input power but doubles τ_{BG} leading to only a fourfold decrease in effective photon detection probability at the signal's arrival time. Therefore, in case 2 with the input ND filter, the total attenuation at the time instant of the signal is smaller, and the SNR is better. Another better way to implement the input attenuation is to limit the input optics aperture, which simultaneously improves the depth of field. In this demonstration measurement setup, an ND filter was used instead since an external aperture introduced a field stop. In the shady part of the scene, the SNR is worse with input signal attenuation, although it is still considerably sufficient for detection. Later gating (case 3) helps in sunny and shady conditions but disables measurement of short distances.

B. Measurement Precision

The pixelwise precision for the same measurement scene as in Fig. 3 (in slightly higher 80 klux ambient light) was calculated by doing fifty 3-D measurements and calculating the pixelwise rms values of distance measurement variations. The distance measurements were based on the signal peak positions after processing the histograms as in [15], [17]. The precision follows the expectations: for example at the center of the FOV in the
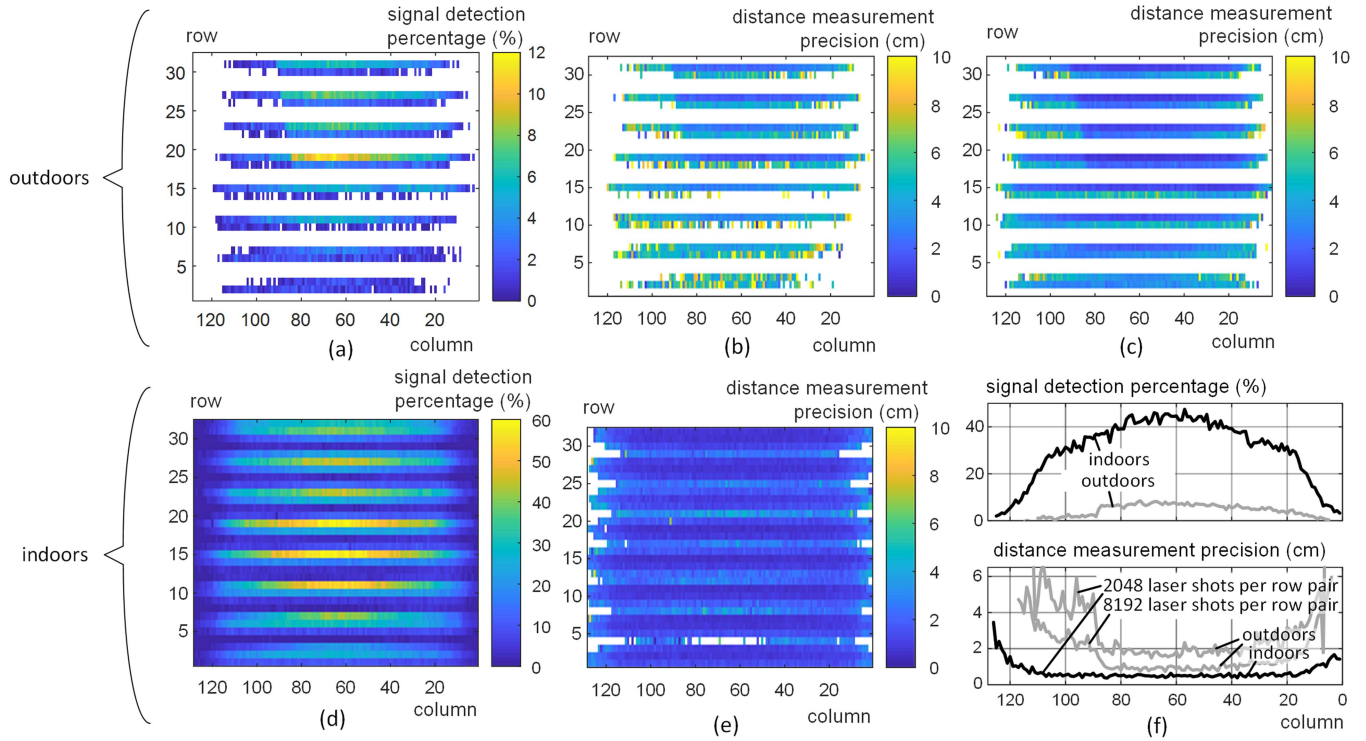
Fig. 6. (a) Signal detection percentages for a white, partially shaded wall (80 klux in the sunny part) at 9.5 m, 0.4 ND filter at input. (b) Distance measurement precision with 15 Hz equivalent frame rate (2048 laser shots per row pair) and (c) 4 Hz equivalent frame rate (8192 laser shots per row pair). (d) Signal detection percentages for a white wall indoors (∼300 lux) at 9.5 m, no ND filter at input. (e) Distance measurement precision for the indoors measurement of (d) with 15 Hz equivalent frame rate (1024 laser shots per row pair, all pixels enabled). (f) Signal detection percentages and distance measurement precisions for row number 27. Gating started at 7 m in all measurements in this figure.
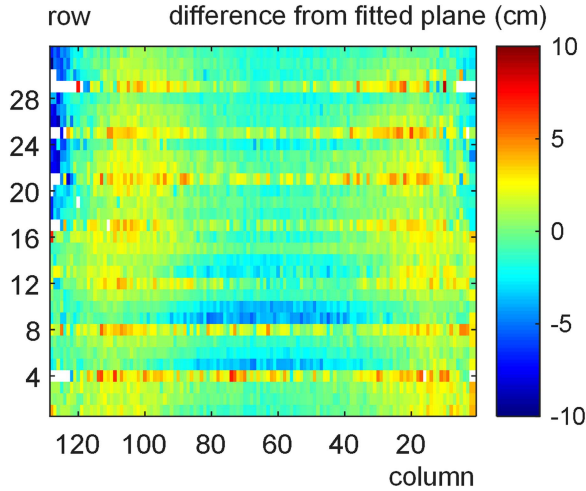

Fig. 7. Measurement accuracy of individual pixels obtained by comparing the 3-D measurement result of a flat white wall indoors at 9.5 m to a fitted plane.

shady part, the signal detection rate is about 12% (Fig. 6(a)) and the precision at the corresponding region in Fig. 6(b) with 2048 laser pulses is about 1.6 cm which is slightly larger than $\sigma_{laser}/\sqrt{N_{signal\_hits}}$, where σ_{laser} is the laser pulse sigma value and N_{signal_hits} is the number of SPAD signal counts (2048·0.12 = 246), and the laser pulse is approximated by a Gaussian pulse shape with a sigma value of FWHM/2.35. The measured precision is slightly higher than the above formula due to the high background noise count rate. Four times more laser pulses per SPAD were used in the measurement result of Fig. 6(c)

(3.8 Hz eq. frame rate) leading to approximately $\sqrt{4} = 2$ times better distance measurement precision for all pixels, which can be seen in Fig. 6(f) showing the signal detection percentages and measured precisions for one line of the SPAD detector matrix.

Indoors, the signal detection rate is higher (Fig. 6(d)) due to a very large τ_{BG} for all pixels and therefore only a very small percentage of background counts blocking signal detection. In such conditions all SPAD rows pairs can be sequentially measured as stray light from the illuminated SPAD rows provides sufficient signal detection percentages and corresponding measurement precision (Fig. 6(d)–(f)). Indoors, the background noise count rate is usually much lower and therefore the precision values are very close to $\sigma_{laser}/\sqrt{N_{signal\_hits}}$.

C. Measurement Accuracy

The accuracy of the measurement was tested by comparing the 3-D measurement result of a flat wall measured indoors to a mathematically fitted plane. In this measurement all SPAD row pairs were sequentially measured. The results in Fig. 7 show that the accuracy error is larger, up to about ±5 cm especially on SPAD rows relying on "stray" laser illumination (first, fourth, fifth, eighth, ninth row, etc.) and within a few cm in the main illuminated SPAD row pairs. This effect likely stems from the temporal differences of the laser diode modes. That is, both of the laser diode types used had a TEM10 type of far-field distribution parallel to the pn junctions, with possibly differing pulse shapes in different far-field directions leading to accuracy error especially near the edges of the emission lobes.

TABLE I
COMPARISON WITH STATE-OF-THE-ART SOLID-STATE SPAD DIRECT TOF 3D IMAGERS

Parameters	Units	This work	[27]	[22]	[21]
transmitter configuration		8 edge emitters, stripe illumination	flood	8 VCSEL elements, block illumination	flood
repetition rate	MHz	0.25	-	5	10
average power	mW	30	9.3	150	90
wavelength	nm	905	905	940	940
receiver technology		0.35 μm CMOS	110 nm CMOS	180 nm BCD	65 nm stacked CMOS
pixel array		128×32[a]	64×64	128×128[b]	240×160
pixel pitch	μm	40	48	25	16
number of TDCs		257	4096	32	600
fill factor	%	35	12.9	18	50
system FOV	deg	40×10	25×25	36x36	63×41
max. distance	m	10	8.2	15	4/13.5
background light	klux	50/indoors	30	indoors	10/indoors
optical filter bandwidth	nm	43	10	-	-
frame rate	frames/s	15	25	1	20
3D precision	σ, cm	1.5…5/0.5…3[c]	3…27[d]	-	-/0.1…1.1
pulse width	ns	2	20	1-2	1.5
accuracy	cm	±2…5[c]	±15	+/-10[f]	±1.5

[a]Bandpass filter cutting off edgemost rays. [b]The receiver has 32 TDCs for 2048 SPADs, a machine learning based algorithm is used to upscale the spatial resolution. [c]Measured at a distance of 9.5 m. [d]Excluding pile-up distortion. [f]Measured at a distance of 15 m.

IV. DISCUSSION

We have shown that the stripe-based illumination approach allows one to achieve a measurement range of ∼10 m at a spatial resolution of ∼16 × 128 pixels (FOV 40° × 10°) and frame rate of 15 frames/s and cm-level precision in a relatively high background illumination condition (∼50 klux) to non-cooperative targets with a relatively low average illumination power of ∼30 mW. At low background illumination levels, the full spatial resolution of the receiver (32 × 128 pixels) can be utilized. In the presented design, illumination stripes were used contrary to earlier designs which focused on achieving homogenous illumination blocks [15], [16]. The use of stripes increases the irradiance at the illuminated target points improving thus the SNR, although at the price of reduced spatial resolution, especially at long ranges. It was also shown that the homogeneity of the optical beam (i.e., variation of laser pulse shape within the far-field) may have an effect on the achievable accuracy.

The block-based illuminator was realized using 8 edge-emitting laser diodes, each operating at a pulse energy of ∼110 nJ and a pulse width of ∼2 ns. The obvious way to improve the performance would be to increase the pulse energy and/or to increase the number of illumination blocks. This is not however a straightforward solution due to the performance limitations of high speed and high power laser drivers and the increasing complexity of the laser diode based transmitter (using separate edge emitters or a VCSEL with addressable sub-units).

From the receiver point-of-view, the use of multi-hit time-to-digital converters (TDC), a macro-pixel SPAD approach and on-chip histogramming would certainly improve the performance allowing maximum receiver aperture (input optical attenuation would not be needed) and real-time processing of the results [7], [8], [21], [26], [27].

Table I presents a summary of a few recent solid-state 3-D range imager realizations. The present work seems to compare well with the state of the art, although detailed comparison is difficult since not all parameters are reported in the papers. The work in [27] uses counts from nearby SPADs to validate SPAD counts to achieve comparable 3-D measurement range, FOV and frame rate as in this work, although in lower background illumination conditions, and has a very wide 20 ns laser pulse which might lead to significant pileup-effects. Interestingly, [27] demonstrates also on-chip sensitivity adjusting techniques for performance optimization. Reference [22] uses a somewhat similar type of illumination scheme as in the present work: an addressable VCSEL array to illuminate the scene sequentially with eight rectangular areas. The illuminated areas are comparatively larger, illumination is focused on the FOV of 16 × 128 SPAD detectors at a time compared to 2 × 128 SPAD detectors in the present work. Our present work has eight times more TDCs compared to [22], sufficient to measure all illuminated SPADs at a time. The stacked CMOS technology used in [21] enables a large number of TDCs but could perform better with a rolling illumination scheme, although a more complicated illumination scheme compared to the present work would be needed due to multiple clusters of simultaneously operating SPAD subgroups. A recent study focusing on the improvements of the histogram data processing and SPAD biasing approaches claims to achieve an accuracy and range of 10 cm and 10 m, respectively, in 70 klux background illumination at a frame rate of 20 frames/s with a spatial resolution of 32 × 32 pixels. The optical signal power used is however much higher, i.e., the average power for a single pixel is 4.5 mW [14], whereas in the present study the average illumination power for the whole system FOV is ∼30 mW.

The conclusion of the work is that the sequential illumination of the system FOV may pave the way for improved performance in the solid-state 3-D pulsed time-of-flight SPAD based range imaging. Focusing of the illumination blocks into stripes further increases the performance, albeit at the price of lower spatial resolution.

REFERENCES

[1] B. Schwarz, "Mapping the world in 3D," *Nature Photon.*, vol. 4, no. 7, pp. 429–430, Jul. 2010.

[2] V. C. Coffey, "Imaging in 3-D: Killer apps coming soon to a device near you!," *Opt. Photon. News*, vol. 25, no. 6, pp. 36–43, Jun. 2014.

[3] R. Lange and P. Seitz, "Solid-state time-of-flight range camera," *IEEE J. Quantum Electron.*, vol. 37, no. 3, pp. 390–397, Mar. 2001.

[4] C. S. Bamji et al., "A 0.13 um CMOS system-on-chip for a 512 × 424 time-of-flight image sensor with multi-frequency photo-demodulation up to 130 MHz and 2 GS/s ADC," *IEEE J. Solid State Circuits*, vol. 50, no. 1, pp. 303–319, Jan. 2015.

[5] M. A. Albota et al., "Three-dimensional imaging laser radar with a photon counting avalanche photodiode array and microchip laser," *Appl. Opt.*, vol. 41, pp. 7671–7767, Dec. 2002.

[6] C. Niclass, A. Rochas, P.-A. Besse, and E. Charbon, "Design and characterization of a CMOS 3-D image sensor based on single photon avalanche diodes," *IEEE J. Solid-State Circuits*, vol. 40, no. 9, pp. 1847–1854, Sep. 2005.

[7] M. Perenzoni, D. Perenzoni, and D. Stoppa, "A 64 x 64-Pixels digital silicon photomultiplier direct TOF sensor with 100-MPhotons/s/pixel background rejection and imaging/altimeter mode with 0.14% precision up to 6 km for spacecraft navigation and landing," *IEEE J. Solid-State Circuits*, vol. 52, no. 1, pp. 151–160, Jan. 2017.

[8] S. W. Hutchings et al., "A reconfigurable 3-D-stacked SPAD imager with in-pixel histogramming for flash LiDAR or high-speed time-of-flight imaging," *IEEE J. Solid-State Circuits*, vol. 54, no. 11, pp. 2947–2956, Nov. 2019.

[9] H. Ruokamo, L. W. Hallman, and J. Kostamovaara, "An 80 × 25 pixel CMOS single-photon sensor with flexible on-chip time gating of 40 subarrays for solid-state 3-D range imaging," *IEEE J. Solid-State Circuits*, vol. 54, no. 2, pp. 501–510, Feb. 2019.

[10] D. Bronzi, Y. Zou, F. Villa, S. Tisa, A. Tosi, and F. Zappa, "Automotive three-dimensional vision through a single-photon counting SPAD camera," *IEEE Trans. Intell. Transp. Syst.*, vol. 17, no. 3, pp. 782–795, Mar. 2016.

[11] F. M. Della Rocca et al., "A 128 × 128 SPAD motion-triggered time-of-flight image sensor with in-pixel histogram and column-parallel vision processor," *IEEE J. Solid-State Circuits*, vol. 55, no. 7, pp. 1762–1775, Jul. 2020.

[12] A. Eshkoli and Y. Nemirovsky, "Characterization and architecture of monolithic N+P-CMOS-SiPM array for ToF measurements," *IEEE Trans. Instrum. Meas.*, vol. 70, 2021, Art. no. 2002909.

[13] L. J. Koerner, "Models of direct time-of-flight sensor precision that enable optimal design and dynamic configuration," *IEEE Trans. Instrum. Meas.*, vol. 70, 2021, Art. no. 8502609.

[14] D. Li, R. Ma, X. Wang, J. Hu, and Z. Zhu, "Optimization of system design and calibration algorithm for SPAD-based LiDAR imager," *IEEE Trans. Instrum. Meas.*, vol. 71, 2022, Art. no. 2006010.

[15] J. Kostamovaara, S. Jahromi, L. Hallman, G. Duan, J.-P. Jansson, and P. Keränen, "Solid-state pulsed time-of-flight 3-D range imaging using CMOS SPAD focal plane array receiver and block-based illumination techniques," *IEEE Photon. J.*, vol. 14, no. 2, Apr. 2022, Art. no. 6817911.

[16] S. Jahromi, J.-P. Jansson, P. Keränen, and J. Kostamovaara, "A 32 × 128 SPAD-257 TDC receiver IC for pulsed TOF solid-state 3-D imaging," *IEEE J. Solid-State Circuits*, vol. 55, no. 7, pp. 1960–1970, Jul. 2020.

[17] J. Kostamovaara, S. Jahromi, and P. Keränen, "Temporal and spatial focusing in SPAD-based solid-state pulsed time-of-flight laser range imaging," *Sensors*, vol. 20, no. 21, Oct. 2020, Art. no. 5973.

[18] L. W. Hallman, S. Jahromi, J.-P. Jansson, and J. Kostamovaara, "On two-dimensional rangefinding using a ∼1 nJ/∼100 ps laser diode transmitter and a CMOS SPAD matrix," *IEEE Photon. J.*, vol. 10, no. 4, Aug. 2018, Art. no. 6802712.

[19] I. Niskanen et al., "Time-of-flight sensor for getting shape and motion model of automobiles toward digital 3D imaging approach of autonomous driving," *Automat. Construction*, vol. 121, Oct. 2020, Art. no. 103429.

[20] M. Immonen et al., "Fusion of 4D point clouds from a 2D profilometer and a 3D LiDAR on an excavator," *IEEE Sensors J.*, vol. 21, no. 15, pp. 17200–17206, Aug. 2021.

[21] C. Zhang et al., "A 240 × 160 3D-stacked SPAD dToF image sensor with rolling shutter and in pixel histogram for mobile devices," *IEEE Open J. Solid-State Circuits Soc.*, vol. 2, pp. 3–11, 2022.

[22] S. Zhuo et al., "Solid-state dToF LiDAR system using an eight-channel addressable, 20-W/ch transmitter, and a 128 × 128 SPAD receiver with SNR-based pixel binning and resolution upscaling," *IEEE J. Solid-State Circuits*, vol. 58, no. 3, pp. 757–770, Mar. 2023.

[23] J. Kostamovaara et al., "On laser ranging based on high-speed/energy laser diode pulses and single-photon detection techniques," *IEEE Photon. J.*, vol. 7, no. 2, Apr. 2015, Art. no. 7800215.

[24] G. Fouche, "Detection and false-alarm probabilities for laser radars that use geiger-mode detectors," *Appl. Opt.*, vol. 42, no. 27, pp. 5388–5398, Sep. 2003.

[25] M. Henriksson, "Detection probabilities for photon-counting avalanche photodiodes applied to a laser radar system," *Appl. Opt.*, vol. 44, no. 24, pp. 5140–5147, Aug. 2005.

[26] A. R. Ximenes, P. Padmanabhan, M.-J. Lee, Y. Yamashita, D.-N. Yaung, and E. Charbon, "A modular, direct time-of-flight depth sensor in 45/65-nm 3-D-stacked CMOS technology," *IEEE J. Solid-State Circuits*, vol. 54, no. 11, pp. 3203–3214, Nov. 2019.

[27] E. Manuzzato, A. Tontini, A. Seljak, and M. Perenzoni, "A 64×64-pixel flash LiDAR SPAD imager with distributed pixel-to-pixel correlation for background rejection, tunable automatic pixel sensitivity and first-last event detection strategies for space applications," in *Proc. IEEE Int. Solid-State Circuits Conf.*, 2022, pp. 96–98.